National Aeronautics and
Space Administration

Science Mission Directorate
SMD-LUN-102
REVISION A
RELEASE DATE: MAY 25, 2025

SCIENCE MISSION DIRECTORATE (SMD) EXPECTED VOLATILES AND DUST HAZARDS IN ARTEMIS III AND IV SAMPLES

Barbara Cohen, NASA’s Goddard Space Flight Center
Jennifer Heldman, NASA’s Ames Research Center
Dana Hurley, John Hopkins University Applied Physics Laboratory
Rostislav Kovtun, Amentum
Brett Denevi, John Hopkins University Applied Physics Laboratory
Angela Garcia, Amentum
Juliane Gross, NASA’s Johnson Space Center
Andrew Needham, NASA’s Goddard Space Flight Center

REVISION AND HISTORY PAGE

Revision No.	Change No.	Description	Effective Date
-	-	Initial Release	05/15/2023
A		Updated Title to include Volatiles and Dust Hazards. Updated content to include water estimates for polar regions, subsurface temperatures, and dust particle-size frequency distributions. This version was approved at the SHECB for SMD.	5/25/2025

TABLE OF CONTENTS

SECTION **PAGE**

APPENDICES

1.0 INTRODUCTION

1.1 PURPOSE

One of NASA’s Moon to Mars Objectives is to determine the distribution, abundance, and composition of lunar volatiles. These volatiles have been detected from orbital instrumentation, but much is still unknown regarding details of how abundance and composition varies with location. The purpose of this document is to summarize what is known regarding composition of volatiles that might be encountered by crew during Artemis surface operations, to address concerns regarding development of hardware for sample collection and preservation, as well as regarding understanding the safety risks of bringing collected volatile-bearing samples back into a crewed cabin.

Initial assessments of what returning volatiles could look like used volatile abundance and composition data returned from the LCROSS mission, which characterized one of the deepest, coldest permanently shadowed regions on the Moon. However, these data are not necessarily applicable to locations where Artemis crew will explore, driving potentially unnecessary levels of hazard control, which in turn may affect volatile container design and how much sample can be returned. This document informs on the volatile composition and abundance in samples likely to be collected by crew during the Artemis III mission to the lunar south polar region.

1.2 SCOPE

This document provides the geologic context and current understanding of volatile stability and accumulation in micro cold traps expected to be accessible on the Artemis III mission. This document provides assessments from Apollo and subsequent data that suggest a low likelihood of sampling volatile species that could pose hazards to crew. Finally, this document provides a list of the volatile compounds that could be present in the samples we expect to take on Artemis III and the abundance of those volatiles.

1.3 CHANGE AUTHORITY/RESPONSIBILITY

NASA Office of Primary Responsibility (OPR) identified for this document is Science Mission Directorate (SMD) Exploration Science Strategy and Integration Office (ESSIO). Proposed changes to this document shall be submitted via a Change Request (CR) to SMD ESSIO for consideration and disposition.

2.0 DOCUMENTS

2.1 APPLICABLE DOCUMENTS

The following documents include specifications, models, standards, guidelines, handbooks, and other special publications. The documents listed in this paragraph are applicable to the extent specified herein.

Document Number	Document Title

2.2 REFERENCE DOCUMENTS

The following documents contain supplemental information to guide the user in the application of this document. Additional references to data sources in this document can be found in Appendix C.

Document Number	Document Title
CaRI 010	Contamination and Research Integrity (CaRI) Team Adjudication on Lunar Volatiles

3.0 DEFINITIONS AND ASSUMPTIONS

3.1 DEFINITIONS

Here we define terms relevant to this document.

Lunar regolith: The fragmental and unconsolidated rock material that covers the entire lunar surface. This layer is the result of the continuous impact of meteoroids and the steady bombardment of charged particles from the sun and stars. The regolith is generally about 4-5 m thick in mare regions and 10-15 m in highland areas and contains all sizes of material from large boulders to sub-micron dust particles.

Lunar soil: Lunar soil is defined as the subcentimeter fraction of the regolith. However, it is commonly used interchangeably with regolith. Lunar soil contains no organic matter and is not formed through biologic or chemical means as terrestrial soils are, but strictly through mechanical comminution from meteoroids and interaction with the solar wind and other energetic particles.

Lunar dust: Refers specifically to particles in the soil or regolith that are ~10 microns in diameter or smaller.

Volatiles: Compounds that exist primarily as vapor or liquid at and above Earth ambient conditions (20°C or 293K, 1 bar atmosphere) but condense at lower temperatures. On the Moon, these compounds sublimate directly from a solid to a gas due to the low surface pressure.

Permanently Shadowed Region (PSR): Region that does not experience direct sunlight (likely for billions of years).

Transiently Shadowed Region (TSR): Region that only has limited direct sunlight (few days of sun per month).

Cold Trap: Location cold enough that volatile species could be thermodynamically stable at the surface or near subsurface for geologically long timescales. Cold traps can be as small as 1 cm which is the smallest area that can remain cold enough for volatiles due to lateral heat transfer through the regolith.

Stability: The condition where the sublimation rate of a volatile compound is low enough such that ice can exist for geologically long timescales (loss rate of <1 mm/billion years).

Volatile stability at the surface and in the subsurface is primarily driven by peak and minimum surface temperatures over the lunar year. The surface temperature is largely determined by direct photons (sunlight) and secondarily photons reflected and scattered from nearby terrain. The varying topography and resultant scattered light can lead to a gradient in both temperature and lighting in shadowed regions and from the rim to the floor of larger craters. For smaller shadowed regions, lateral heat transfer through the regolith becomes the dominant heat source driving temperature and the minimum cold trap size is ~1 cm; at smaller sizes the lateral heat dominates and the region is too warm for volatile sequestration (Hayne et al. 2015).

Due to these processes influencing the lunar thermal regime, the term “PSR” is not the most useful framework for considering volatile stability, because this terminology conflates lighting and thermal conditions. Instead, in this document we consider thermodynamically favorable regions for volatiles to collect and persist at both poles of the Moon. Temperature is a necessary condition for sequestering volatiles, but cold temperatures does not mean volatiles HAVE to be there, depending on the geologic setting and history.

3.2 ASSUMPTIONS FOR ARTEMIS III AND IV

The Artemis III mission will return samples from a landing site within 6° of the south pole of the Moon, within one of the 13 regions defined by NASA.

Most of the Artemis III samples will be rock and regolith samples that have been or currently are exposed to sunlight, like those collected during Apollo.

The South Polar region is geologically most akin to the Apollo 16 mission, with mature regolith developed over extensively cratered highlands bedrock.

The astronauts will likely go into the coldest area available within the explorable zone and collect a sample to be returned under ambient conditions. These small areas may be places where the local topography protects the surface from incident photons, so the temperature would remain below that of the nearby surface.

4.0 VOLATILES

Understanding the origins, ages, and evolution of lunar polar volatiles are key science objectives that benefit substantially from the use of environmentally controlled sample stowage and curation. Here, “volatiles” refers to compounds such as water, carbon dioxide, methane, etc. that exist primarily as vapor or liquid at and above Earth ambient conditions (20°C or 293K, 1 bar atmosphere) but condense at lower temperatures. On the Moon, the low surface pressure means that these compounds sublime directly from a solid to a gas.

There are multiple potential sources and sinks of lunar volatiles, including contributions from early volcanic outgassing, asteroid impacts, comet impacts, solar wind interactions with regolith, and/or ongoing meteoroid bombardment (see, for example, Anand, 2011; Lucey et al., 2022). Studying these compounds will allow us to determine whether volatiles were emplaced early in Solar System history and are ancient, have been delivered continuously throughout lunar history, or are a recent phenomenon (or some combination of the three). Once the volatiles were emplaced, the volatile deposits likely experienced subsequent modification and evolution. Processes such as solar wind sputtering, cosmic ray-induced chemical reactions, thermal diffusion and lateral heat conduction, and/or orbital effects such as true polar wander (and the resulting volatile migration) may all affect the present-day observed volatile distribution and characteristics. The scientific value in understanding the origins, ages, and evolution of lunar volatiles extends beyond the Moon; understanding volatile delivery history and processes on the Moon is also key for elucidating processes occurring across the Solar System such as on Mars, Mercury, Ceres, asteroids, and ocean worlds.

Studies of lunar polar volatiles are also key to enabling sustained human exploration of the Moon via in situ resource utilization (ISRU). The Artemis missions to the lunar south pole are designed to take advantage of the resources that may be found there, particularly abundant sunlight, favorable thermal conditions, and access to potential stores of water and other volatile compounds. As with terrestrial mining practices, the exploration of such potential resource deposits requires an understanding of the origin of the volatiles, their lateral and vertical distribution, form, and abundance (Cannon and Britt, 2020; Casanova et al., 2020). These fundamental science goals will build the necessary predictive capabilities to enable assessments of lunar volatile resources, such as the replenishment rates, locations, grade, and processing needs, and will allow for optimal design and operation of ISRU architectures and hardware elements.

In addition to the host of community reports, two NASA-commissioned reports, the Artemis III (AIII) Science Definition Team (SDT) Report (Weber et al., 2020) and the Lunar Water ISRU Measurement Study (LWIMS) (Kleinhenz et al., 2020) defined goals for volatiles science and preparation for ISRU, many of which require cold/cryogenic sample return. The goals of the Artemis III SDT and the Artemis III Geology team are considered in this white paper. We note, however, that subsequent landed missions during the ‘sustainable’ phase of Artemis should have increased capabilities for cold sample return (*e.g.,* mass, temperatures, sample volumes, etc.). As such, the considerations for sample collection, type, and nature will change for those missions.

4.1 OBSERVATIONS AND ORIGIN OF LUNAR VOLATILES

The lunar surface at the poles experiences both direct sunlight and indirect radiation from topography – a situation similar to the equatorial sites visited by Apollo, but with muted intensity. A rough guide to the equilibrium surface thermal conditions at the equator vs pole is that fully sunlit surface regolith near the equator experiences temperatures from -150 to +100ºC (123 to 373 K) in shade and sunlight, whereas sunlit polar regions experience -200 to 0ºC (73 to 273 K).

A more granular understanding of the lunar thermal environment comes from the Diviner Lunar Radiometer Experiment aboard NASA’s Lunar Reconnaissance Orbiter (Paige et al., 2010) and models of the poles that account for the solar ephemeris and local topography. These models noted as far back as the 60's that the topography at the poles would be such that direct sunlight would be blocked from some large craters and even some smaller depressions (“permanently shadowed”). Coupled with the low internal heat flow of the Moon measured by Apollo surface experiments, the implication is that the surface temperature in these areas would remain lower than surrounding sunlit regions. This thermal environment could serve as “cold traps,” or regions where volatile species could be stable at the surface or near surface because the long-term average surface temperature is below the sublimation temperature of several volatile species that may have been delivered to the Moon via lunar outgassing, solar wind, or comet and asteroid impact.

Large PSRs can have surface temperatures as low as 40K in their interiors. These interior areas within large craters such as Shoemaker, Faustini, Haworth, and Cabeus, are unreachable under the slope and hazard guidelines for human exploration during the early Artemis missions. However, thermal modeling based on orbital surface temperature measurements suggests that small cold areas may exist at relatively shallow depths (few cm to 10s of cm and deeper) both within and outside of PSRs (Hayne et al., 2021; Zhang and Paige, 2009). These “micro-cold-traps” are on the order of meters in diameter and exist because of shadowing by local lunar topography and are likely to be geologically young features. Micro-cold-traps exist at or near all Artemis III candidate landing regions and sites and are considered important to include in potential EVA activities.

Adsorbed volatile species likely exist in lunar soils at all latitudes and seasons. The solar wind implants protons (H) and noble gases (He, Ne, Ar) into the top 20-30 nm of lunar regolith grains (Wieler, 1998; Wieler, 2016). Water and OH- molecules form during the interaction of the solar wind and cosmic rays with silicates in the regolith (Crites et al., 2011; Dartnell, 2011; Liu et al., 2012; Walker, 1975). From orbit, these OH- or H2O molecules are detectable in the upper micrometer of lunar grains (Clark, 2009; Pieters et al., 2009; Sunshine et al., 2009) across the lunar surface, exhibiting seasonal and possibly even diurnal variabilities.

Condensed volatile species (*i.e.,* ices) are known to occur in the subsurface and surface regolith in polar regions on the Moon. Radar and neutron spectrometer data map hydrogen content (water equivalent hydrogen) Lunar Prospector and LRO neutron spectrometer (NS) results show decreased neutron density at lunar poles – consistent with ~150 ppm enhanced hydrogen - if water ice were confined to PSRs alone, this translates to about 0.5 wt% (Campbell et al., 2003; Feldman et al., 2000; Feldman et al., 2001; Livengood et al., 2018; Mitrofanov et al., 2016; Nozette et al., 1996; Sanin et al., 2017; Sanin et al., 2012). Neutron results are most consistent with a desiccated layer some 10s of cm thick at the surface, and water ice residing below that depth.

The LCROSS mission excavated material to tens of meters of depth in the permanently-shadowed interior of Cabeus crater. This region was targeted because it was observed by the LRO and LP NS as one of the most hydrated regions of the south pole. The onboard spectrometers observed regolith with 5-10 wt.% water, along with other volatile substances, including ammonia and simple carbon compounds (Colaprete et al., 2010; Heldmann et al., 2012). We do not know the exact form of the water ice in these deposits (inter-granular ice, mixed with regolith, etc.), however, future human and robotic missions may help constrain the form and composition of volatiles by measuring the volatiles and probing the regolith geotechnical properties in and around these large PSRs.

Surface volatiles (*e.g.,* frost) have been detected from orbit in patchy regions within some PSRs (Fisher et al., 2017; Hayne et al., 2015; Li et al., 2018). Surface ice distribution is “patchy” rather than contiguous over regions with similar thermal environments. However, ShadowCam has not found any definitive evidence of high albedo associated with water ice frost anywhere within the South Polar region (Ando et al., 2025). Contrast this with Mercury where obvious surface water frost correlates nearly perfectly with thermal contours at the poles (Chabot et al., 2012; Deutsch et al., 2016).

In cold traps, temperature and age are the key drivers that dictate whether volatiles may be present within lunar regolith – that is, geologic terrains that are older and have been kept at lower temperatures can potentially have accumulated a higher abundance and a wider range of volatile compounds (Cannon et al., 2020; Deutsch et al., 2020; Farrell et al., 2019). However, the word “cold trap” itself denotes a supply side issue – molecules must be delivered to these regions to be trapped and accumulate. For this to happen, the supply of water and other volatile molecules from sources must exceed their escape rate, and photodissociative escape must be slow compared to ballistic migration. However, this does not appear to be the case. The LADEE Neutral Mass Spectrometer (NMS) and UltraViolet Spectrometer (UVS) identified the primary atmospheric constituents at altitude, their density, and variability (Benna et al., 2015; Hodges Jr., 2016). Water and OH- were only observed in the exosphere during meteor stream events (Benna et al., 2019), rather than a continual background supply. In addition, the diurnal cycle of argon into the exosphere implies empty bonding sites on lunar surface grains that water should preferentially occupy if supply were available (Hodges, 2002). These results imply that the current lunar surface is largely desiccated and that the Moon is currently in a net volatile-loss regime, rather than net accumulation.

The deep lunar polar volatile locations correlate with a paleopole orientation > 2 billion years old (Siegler et al., 2016). The implication is that the deep volatiles reservoirs on the moon are leftovers from a large, volatile-rich object that impacted the Moon > 2 Ga ago and has been being gardened and lost ever since. This also is consistent with the lack of frost filling all observable PSR cold traps at the lunar surface. Transient exposure and short-scale transport of buried volatiles is more consistent with available observational data than continuous resupply of volatiles (*i.e.,* via ballistic hopping) to polar cold traps.

Adsorption of solar wind-derived volatiles occurs in all lunar soil regardless of surface temperature. The supply of solar wind has been effectively constant throughout geologic time, so more mature (older) lunar regolith contains higher abundances of solar wind volatiles. We know that the south pole of the Moon is some of the oldest terrain on the Moon, similar to what was sampled by Apollo 16, for example. These volatile species can be adsorbed, or loosely bound, to grain surfaces.

4.2 VOLATILES IN APOLLO SAMPLES

The six Apollo missions collected 382 kg of sample, including ~115 kg of regolith, from the equatorial regions of the Moon. The regolith samples included a range of sample types, including:

- Regolith scoops sampling down to 30 cm deep
- Drive Tubes of regolith sampling down to 70 cm deep
- Deep drill regolith cores sampling down to 2.8 m deep
- Vacuum sealed regolith samples collected at the surface (SESC and GASC) and up to ~60 cm depth (CSVC -Core Sample Vacuum Container)
- Apollo regolith samples were returned in (1) sealed ALSRCs (Apollo Lunar Sample Return Container); and (2) Unsealed Sample Containment Bags. Most ALSRCs held a vacuum; they contained a variety of rock & regolith sampling to ~70 cm depth.

Analysis of the gas when the samples were opened showed only trace amounts of solar wind gases (*e.g.,* H, He, Ne, Ar). Historic measurements on GASC and SESC containers also showed only trace amounts of adsorbed solar wind gases. The deep drill core samples, sample equatorial material at cold temperatures down to 2.8 m in depth, were returned unsealed in the Apollo cabin during the multi-day Moon-Earth transit; no adverse effects from those core samples (or the 50+ kg of other unsealed Apollo samples on the Apollos 15-17 missions) were ever reported.

In 2022, gas was extracted for the first time from the CSVC of Apollo 17 sample 73001 that was collected in a double drive tube assembly (73002/73001) on the presumed landslide deposit on the floor of the Taurus-Littrow Valley, at the rim of Lara Crater and the surface expression of the Lee-Lincoln Scarp during the second EVA of the Apollo 17 mission. This 70 cm long double drive tube that was hammered into the surface to record and preserve any potential subsurface stratigraphy and to collect any gasses that may have been emanating from the lunar interior along the Lee-Lincoln scarp.

73001 was the lower part of the drive tube (35-70cm) and was returned inside the CSVC and stored under vacuum inside a secondary sealed container on Earth until it was opened in 2022 as part of the ANGSA (Apollo Next Generation Sample Analyses) initiative. Preliminary analyses of the ANGSA gas showed that trace amounts of H_2O, H_2, CO_2, Ar, and Ne were present. The project is still ongoing; more information can be found in Gross et al. (2025); Parai et al. (2022); and Sharp et al. (2022).

Solar wind gases are some of the most well-studied species in lunar samples. Curran et al. (2020) compiled the abundance of solar-wind gas abundance in rocks and lunar soils. Most of these measurements are made by heating the rocks or soils to release the gases, which is not analogous to the situation under consideration, which is the unconditioned collection and return of samples in the crew capsule. However, several measurements exist for both rocks and soils using low-temperature (100°C) releases for the noble gases, which are reported in Table 1. For nitrogen, Table 1 reports the yield using only mechanical agitation (crushing), without heating (Gibson and Andrawes, 1978). H_2 is difficult to measure in a way that reflects its native (surface) abundance, because of its extreme volatility and propensity to release upon agitation such as during collection. We calculated H_2 abundance (Table 1) as an upper limit from its solar wind ratio to He (Heber et al., 2021).

4.3 ARTEMIS III ENVIRONMENTS

The low angle between the Moon's rotational axis and the normal to the ecliptic plane plus the low inclination of Earth's orbit around the Sun, coupled with lunar topography, enable environmental conditions (including thermal and lighting) that can create thermodynamically favorable regions for volatiles to collect and persist to exist at both poles of the Moon. The Artemis III candidate landing sites are all within the southern highlands within the south polar region. These sites are heavily cratered on ancient terrain undergoing continual impact gardening, which produces relatively young surface topography and extensive regolith mixing (Costello et al., 2021; Denevi et al., 2023; Szalay et al., 2019). The geologically young nature of the present-day terrain indicates that any shadowed regions have not persisted for extensive periods of time and thus have not had adequate time to collect and/or sequester a wide variety of volatile species.

Thermal models based on LRO Diviner temperature measurements provide the best estimate for surface and subsurface temperatures within the candidate Artemis landing regions. The nature of the lunar topography in the south polar region (formation processes and age) is coupled with a physics-based understanding of heat flow and thermal diffusion through regolith, plus contributions from scattered light, are combined to produce the current best estimate of lunar surface and near surface thermal conditions. The resultant understanding of lunar thermal conditions in these regions provides important information for mission planning. For example, shape-from-shading topographic models and Diviner high-resolution models of the lunar surface are useful to show the thermal distribution at specific landing sites. Based on analysis conducted for the Nobile Rim East and Malapert candidate landing sites, the temperatures are expected to remain at or above 100K (±15K) within the 1 km walkback distance of the lander (Fig. 1).

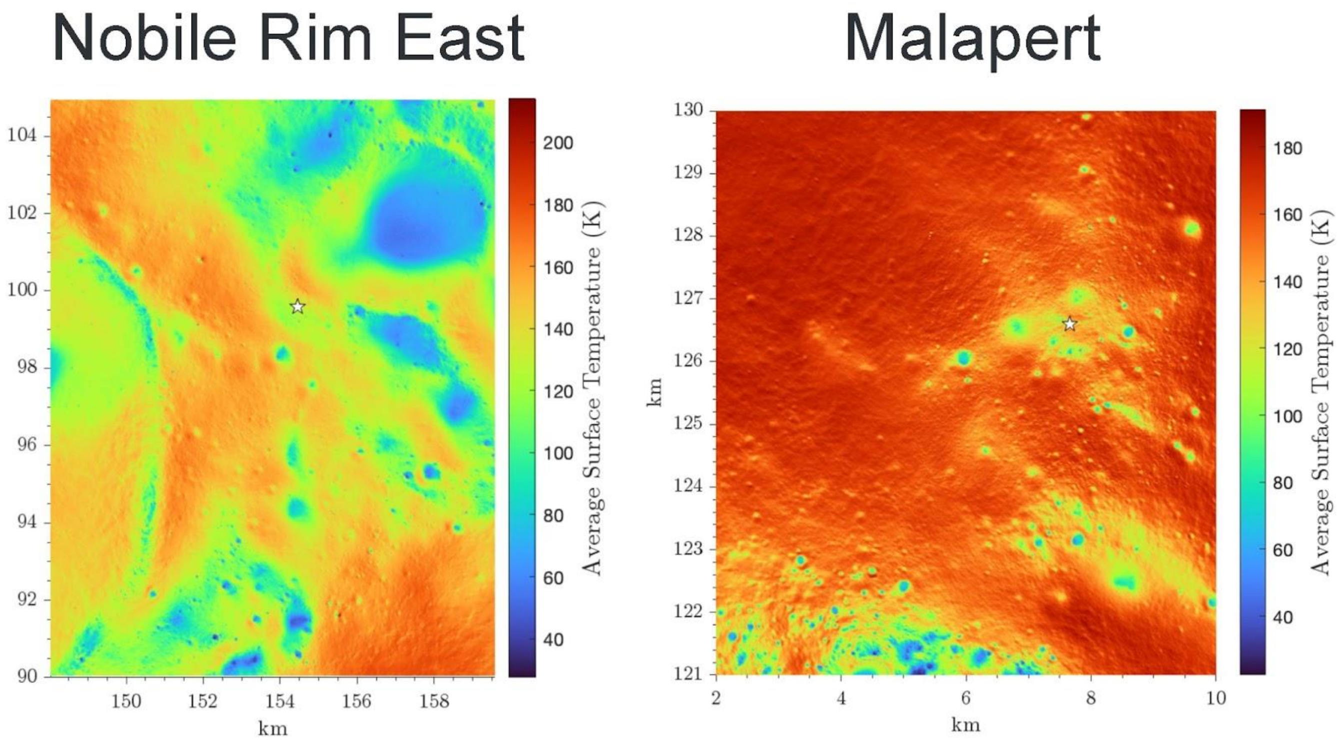

Figure 1. Diviner models for the surface temperature of Artemis III candidate landing regions Nobile Rim East (-83.94S, 57.18E) and Malapert (35.82S, 3.46E). When landing sites are selected, meter-scale models will be made of actual landing sites.

The landing site selection process for Artemis preferentially downselects to regions that do not contain the oldest and coldest PSRs, and as a result the candidate landing sites are expected to not contain these ultra-cold regions. The actual landing site candidates for Artemis III are not available yet, but once available the detailed surface model will be used to predict surface temperatures at these specific sites to validate this preliminary analysis.

The temperature range experienced by these sites would only be stable for solar wind volatiles and water ice; additional volatile species require colder temperatures for sequestration. Figure 2 shows the temperature dependence of volatile stability. For Artemis III, based on using temperature as a proxy for the possibility of volatile sequestration, only solar wind volatiles (also collected during Apollo) and water ice are expected to be encountered within the candidate landing sites and mission constraints (*e.g.,* 1 km walkback distance, surface to ~70 cm depth sampling) for Artemis III.

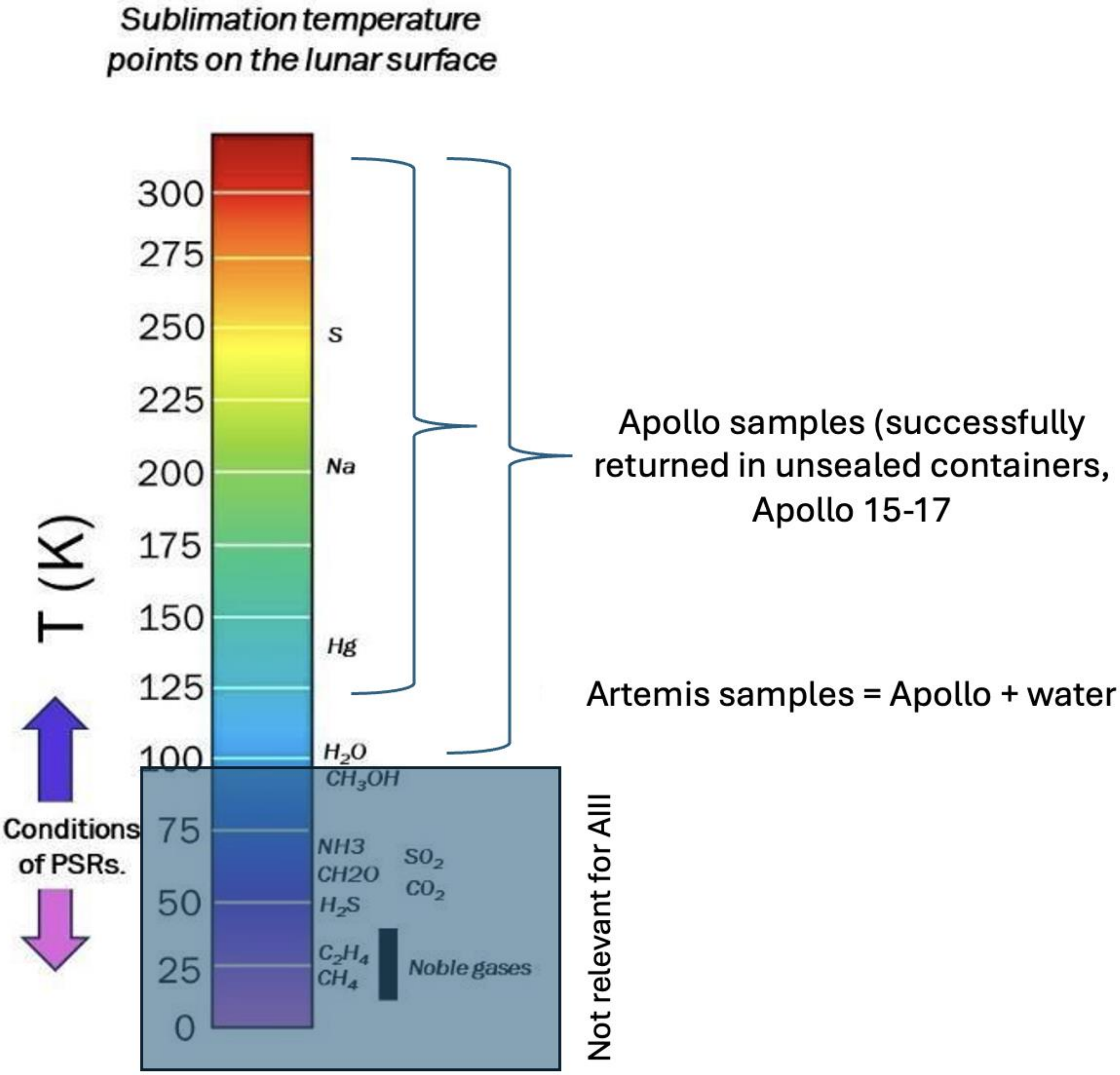

Figure 2. Profile of volatile stability as a function of temperature. Only solar wind volatiles (also collected during Apollo) and water ice are expected to be encountered with Artemis III.

The best upper limit for possible abundance of water at the Artemis landing sites is derived from a cross-correlation between orbital observations of Water Equivalent Hydrogen (WEH) across the lunar south polar regions constrained by the LCROSS measurement of water ice at one location within Cabeus Crater. WEH is measured by the LEND instrument onboard LRO and is sensitive to WEH in the upper ~1 m of the regolith (Sanin et al., 2017). As shown in Figure 3, the LCROSS site contains the highest concentration of WEH in the region at ~0.55%. This WEH corresponds to a measured water ice concentration from LCROSS of 5.6 ± 2.9% by mass (Colaprete et al., 2010). Figure 3 shows that the candidate Artemis landing regions are at half (or less than half) of the LCROSS WEH. Since WEH is our best measurement for water ice concentration, we expect the candidate Artemis landing regions to be able to host less than half of the water abundance measured at the LCROSS site. Therefore, a reasonable assumption for the candidate Artemis landing sites is no more than 2.0% water by mass. However, this is an upper limit. Additional remote sensing data (discussed in Section 4.1) do not suggest elevated levels of surface frost or ice within the Artemis candidate landing zones.

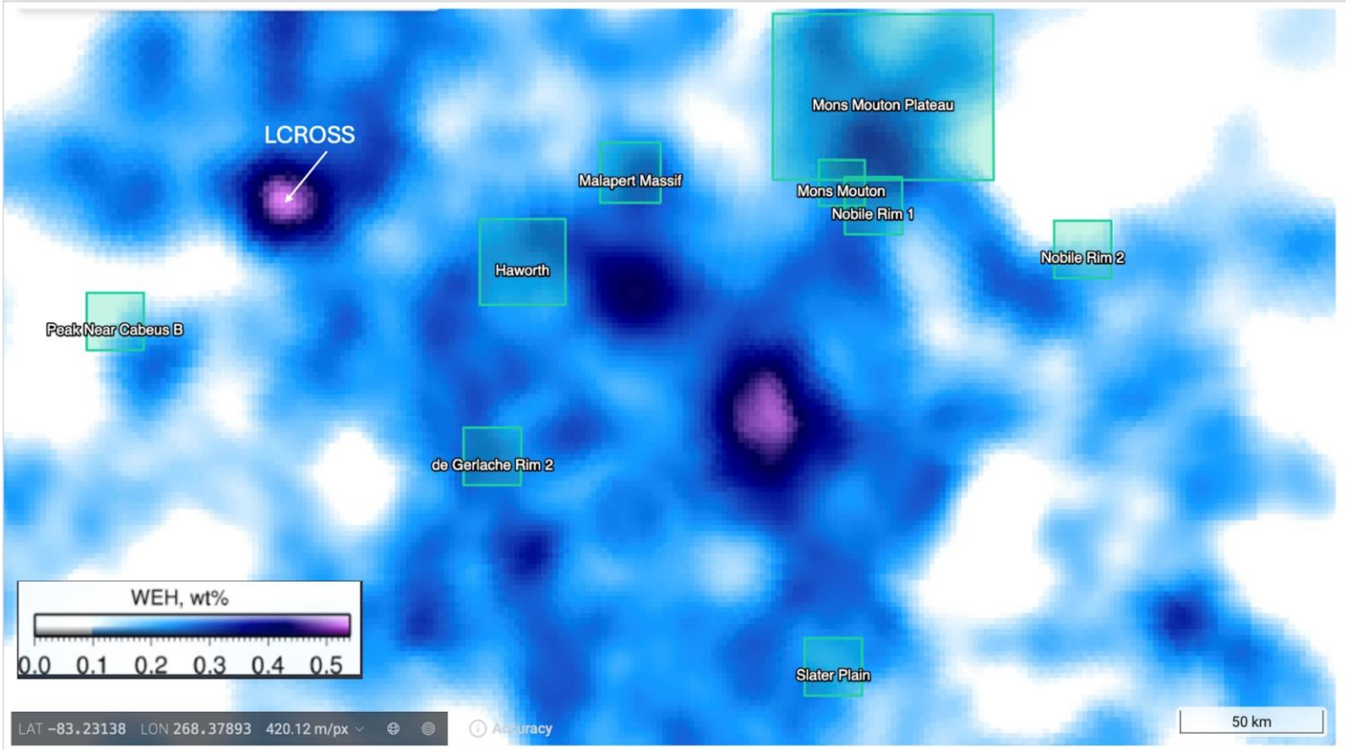

Figure 3. WEH (Water Equivalent Hydrogen) of the south polar regions with the LCROSS impact site and Artemis III candidate landing regions.

4.1 SUBSURFACE TEMPERATURES

The surface temperature changes in response to the lunar day (day-night cycle) and year (seasonal) The thermal signal at the surface propagates into the subsurface to around 50 cm depth (Fig. 4). That means that the lowest annual surface temperature propagates to about 50 cm below the surface. Deeper than that, the subsurface temperature remains constant as a result of a balance between the surface temperature and the Moon's interior heat diffusion. This means that the temperatures below the surface will never be colder than the lowest yearly surface temperature.

At the nearside Apollo sites, the subsurface mean temperatures were ~250K. At the polar regions, the combination of cooler surface temperatures and potentially lower internal heat flow mean that the subsurface material may be somewhat (~10s of degrees) cooler.

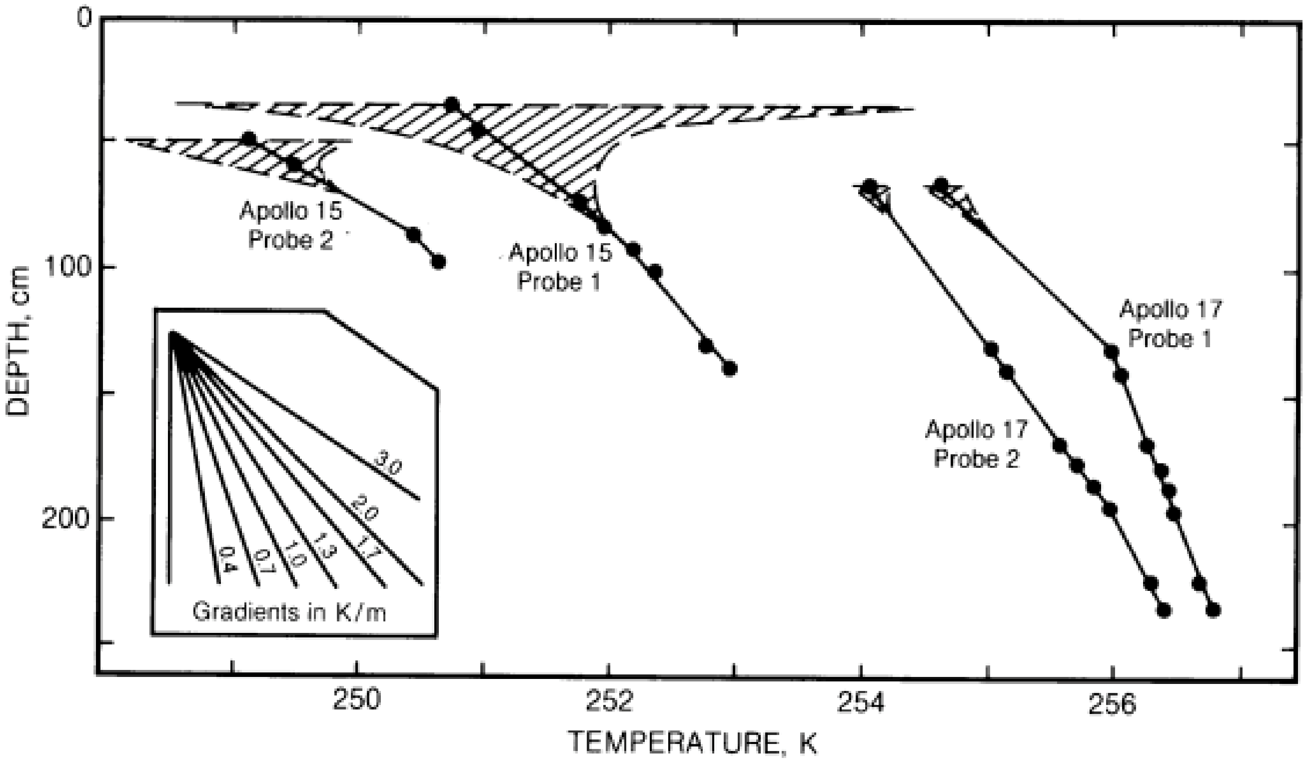

Figure 4. Temperature variation in the lunar subsurface as a function of depth measured at the Apollo 15 and 17 sites. The temperature scale on the x-axis does not capture the wide range of surface temperature variations at the equatorial sites. The hatched areas from 30 to 70 cm depth are the envelopes of day-night variations. Below ~50 cm there is essentially no temperature variation due to the lunar day-night temperature cycles, and the steady temperature gradients recorded are due to internal lunar heat flow (see Ch. 3 in (Heiken et al., 1991).

4.2 HLS CONTRIBUTIONS

In addition to the naturally-occurring solar wind and water expected within the Artemis landing regions, the HLS will also be emitting gases that can potentially be adsorbed or implanted on the upper layer of lunar regolith. The Starship HLS is equipped with six Raptor engines (liquid oxygen + methane) that will be used during launch and much of the landing and ascent phases. Within 100 meters of the lunar surface, HLS plans to use high-thrust landing engines located in the mid-body section of the spacecraft to avoid plume impingement with the lunar regolith. These landing engines burn gaseous oxygen and methane. CH_4/O_2 combustion products are mainly CO_2 and H_2O, whose low molecular weight would cause them to rapidly diffuse over large areas. There may be trace products created from fuel additives or catalysts (as seen in the Apollo samples (Flory and Simoneit, 1972). The exact composition and ratio of the HLS engine fuel and oxidizer is not available at this time but can be incorporated into the analysis of volatiles once provided.

4.3 EXPECTATIONS FOR VOLATILES IN ARTEMIS III AND IV SAMPLES

The presence or absence of volatile compounds depends not only on the surface temperature but also the geologic history of the surface itself and the supply of volatile species over time. As an example, an area might be cold enough for water to be stable, but if no water were delivered to that area in the time it could be stable, the area would be cold but dry. The reason it is important to sample these areas is because it is difficult to create a unique model of geologic history and surface supply. Therefore, we adopt temperature as our primary means of predicting whether volatiles might be present.

For hazard analysis, we assume volatiles would be present in the maximum ratios and abundances that could be stable under the thermal regime. These abundances are in Table 1.

Table 1. Volatile species and abundance that may be present in Artemis III returned samples.

Species	Rocks (cc/g)	Regolith (cc/g)	Source	Samples
H_2	2.14E-03	5.76E-03	Solar Wind	All
^{4}He	4.28E-05	1.15E-04	Solar Wind	All
^{20}Ne	8.30E-08	2.76E-07	Solar Wind	All
^{40}Ar	6.68E-07	2.75E-07	Solar Wind	All
N_2	5.00E-09	1.90E-07	Solar Wind	All
H_2O	trace	2.52E-02	Polar cold trapping + Combustion	Sealed
CO_2	trace	2.00E-07	Combustion	All

5.0 DUST

5.1 ARTEMIS GEOLOGIC SETTING

The Apollo 16 landing site was the only Apollo site in purely highlands terrain, where the surface is older, lighter in color, and more heavily cratered, in contrast to the darker basalts of the maria. The Cayley plains and Descartes mountains are Imbrian in age, significantly older than the surfaces at the other Apollo sites on younger mare features (Hodges and Muehlberger, 1981). The lunar south polar sites under consideration for the Artemis III and IV landing sites are in areas that are at least as old as the Apollo 16 site, if not older (Boazman et al., 2022; Spudis et al., 2008). Therefore, we use the known geologic processes in play at the Apollo 16 site as a proxy for the Artemis III and IV sites.

The processes that create the lunar regolith, impacts and space exposure, comminute (or break up) particles in the regolith over time, a process called maturation. Lunar soil evolves over time as it is exposed to the harsh environment of space. Continuous impacts result in finer grain sizes as a soil “matures”. However, the destructional process of comminution is balanced by the constructional process of agglutinate formation, allowing mature soils to eventually reach a steady state particle size distribution (McKay et al., 1974).

Bulk regolith or soil samples collected in sealed and unsealed containers will contain the full range of particle sizes including lunar dust, or particles <10 μm in diameter, that can represent a hazard to humans via inadvertent inhalation. The fraction of particles at or below this size threshold is an important consideration. We use Apollo 16 returned regolith samples as the clearest analogy to lunar polar regolith to calculate this relevant size fraction.

5.2 PARTICLE SIZE DISTRIBUTION IN APOLLO 16 SAMPLES

The mean grain size of typical lunar soils ranges from 40-800 µm with most falling between 45-100 µm (McKay et al., 1991). In terrestrial terms, most lunar regolith samples would correspond to pebble- or cobble-bearing silty sands, however, it is difficult, and probably dangerous, to apply such terrestrial terminology to lunar soils because their formation mechanisms are so different. Generally, about 10% of lunar soil is greater than 1 mm, about 50% is greater than 100 µm, and about 90% is greater than 10 µm.

The generalized particle size distribution (PSD) curve of lunar regolith has been previously constrained to encompass the <1 cm soil size fraction of surficial and subsurface Apollo samples (Carrier, 2003; Graf, 1993). These distribution curves do not include the pebble-sized rock fraction of the regolith samples that was sieved out by the Lunar Sample Laboratory Facility at NASA JSC as part of the lunar sample curation process. The separation and cataloging of samples into a finer (*i.e.,* <1 cm – soil) and coarser (>1 cm – *e.g.,* unconsolidated regolith, polymict breccia, cataclastic anorthosite, etc.) size fraction has led to confusion on how to bound the physical characteristic of the lunar regolith, both for simulant manufacturing and engineering testing and modeling purposes.

Recent work to incorporate the sieved out >1 cm coarse-grained fraction provides a more comprehensive characterization of surficial lunar regolith grain sizes (Kovtun et al., 2024). The accumulated subsample masses by size fraction that were missing because of curatorial processing were back added to previously tabulated sieve data (wt% by sieve size in microns) to produce new comprehensive PSDs. This study produced a composite, lunar highlands-specific particle size distribution based on 25 surficial Apollo 16 regolith samples (Fig. 4). These samples were selected for their compositional congruity with the surface materials anticipated to be encountered in the lunar south polar region, the focal point of near-future Artemis missions. Additionally, this dataset solely reflects surface samples to disentangle potential noise in trends between surficial, near-surface, and sub-surface samples. A qualitative check was performed on the relativeness of the back added PSD datapoints by reviewing the context under which the pertinent samples were sampled, processed, and catalogued. Furthermore, to create an upper limit particle size threshold for the dataset, a careful review of photographs and measurements of the coarse fraction (*i.e.,* rocks, pebbles < 1cm) was required.

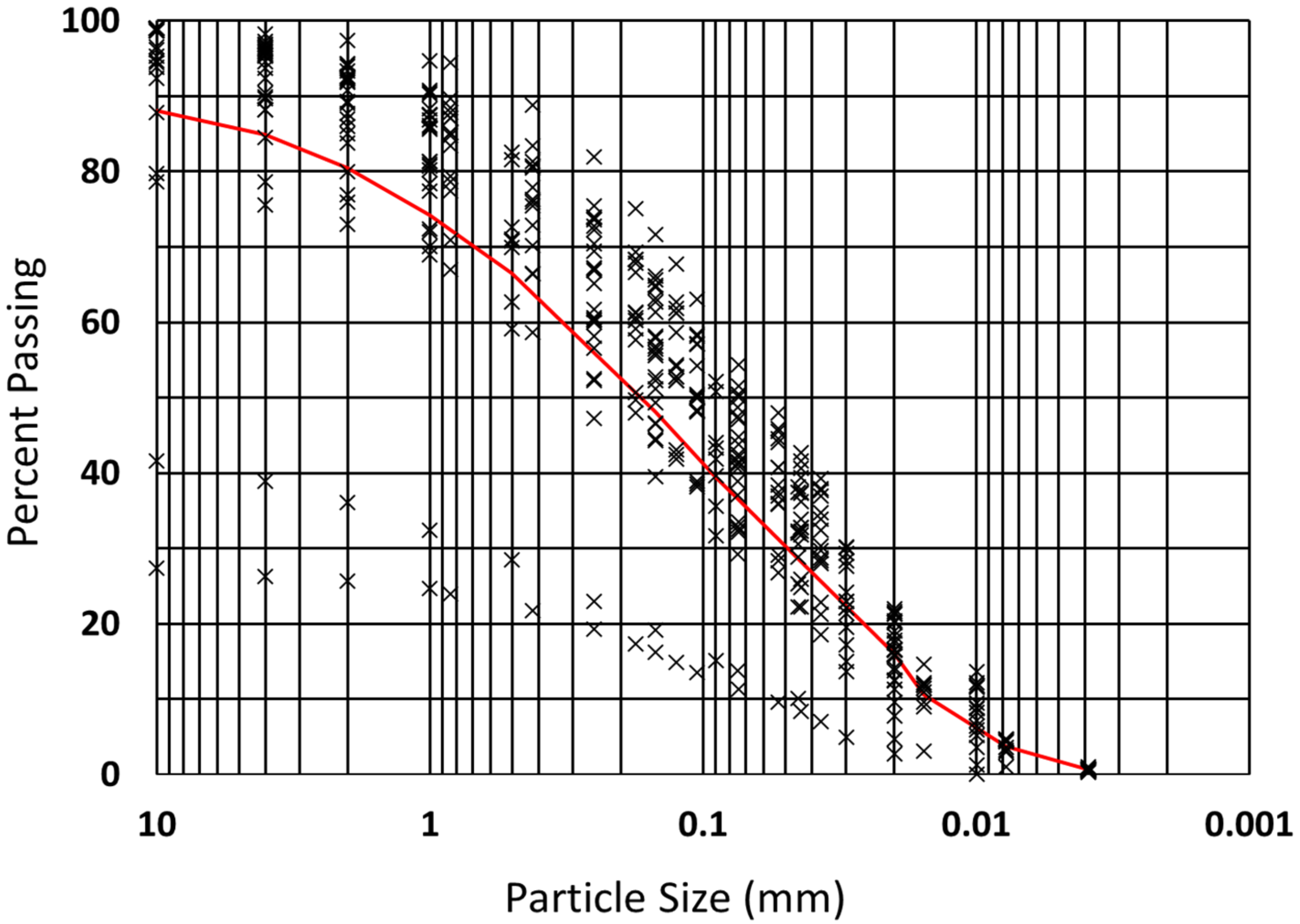

Figure 4. Apollo 16 soil sample particle size distribution with red curve as the average distribution (Kovtun et al., 2024).

5.3 EXPECTATIONS FOR DUST IN ARTEMIS III AND IV SAMPLES

Based on the careful work to fully reconstruct the particle size distribution of Apollo 16 bulk lunar regolith, we recommend the fractions in Table 2 for particle size-based assessments, including lunar dust toxicology assessments.

Table 2. Bulk regolith abundance as weight % by sieve size (cumulative)

Particle size threshold (μm)	**Amount (wt%)**
<500	71.2 %
<10	7.9 %

6.0 FINDINGS

Based on extensive study of Apollo samples, the volatile budget of regolith is likely to be dominated by adsorbed solar wind gases (H, N, and noble gases). Because of the unique thermal regime of the South Polar region, regolith samples could contain more significant amounts of water than the Apollo samples.

The thermal regimes relevant to Artemis III are not cold enough or geologically old enough to support the stability of other volatile species other than water. Based on our best current knowledge, compounds of concern to human health (*e.g.,* CH_4, H_2S, etc.) cannot exist in significant amounts in the Artemis III landing sites or samples.

The Artemis III EVA plan includes visiting the coldest available area in the landing site and collecting regolith samples to test models of volatile origin and distribution. Based on thermal analysis of candidate landing sites, the coldest accessible areas are in the thermal regime where they could retain enhanced amounts of water but are not stable to more volatile compounds. Such samples may be expected to contain additional water and should be collected in sealed containers to maximize their science value.

Sample return from colder regions will require additional analysis and planning. Data from the LCROSS mission, future experiments that would make measurements, and initial results of Artemis III and Artemis IV samples will help constrain the issues associated with sample return from these locations.

Bulk regolith samples collected in sealed and unsealed containers will contain lunar dust. We recommend using the Apollo 16 lunar regolith average of 7.9 wt% of the bulk sample as the fraction that is 10 μm or smaller.

APPENDIX A
ACRONYMS AND ABBREVIATIONS

TABLE A1-1 ACRONYMS

AIST	Artemis Internal Science Team
ALSRC	Apollo Lunar Sample Return Container
ANGSA	Apollo Next Generation Sample Analysis Program
CSVC	Core Sample Vacuum Container
EVA	Extravehicular Activity
GASC	Gas analysis sampling container
ISRU	*In Situ* Resource Utilization
LADEE	Lunar Atmosphere Dust and Environment Explorer
LCROSS	Lunar Crater Observation and Sensing Satellite
LPNS	Lunar Prospector Neutron Spectrometer
LRO	Lunar Reconnaissance Orbiter
LWIMS	Lunar Water ISRU Measurement Study
NMS	Neutral Mass Spectrometer
NS	Neutron Spectrometer
PSR	Permanently Shadowed Region
S&MA	Safety & Mission Assurance
SESC	Special Environment Sample Container
UVS	UltraViolet Spectrometer
VIPER	Volatiles Investigating Polar Exploration Rover

APPENDIX B: SUPPORTING CALCULATIONS FOR EHMST

Total lunar sample mass = 47.5 kg of rocks and regolith (half the allocated utilization mass)

Individual samples will be contained in either a sealed container or an unsealed Teflon sample bag. Maximum volume or mass per sample = 2 kg of regolith in a small sample bag; 1 kg of bulk regolith in a drive tube container.

Unsealed bags:

- Unsealed bags can contain bulk regolith, sieved rake samples, or individual rocks.
- Multiple unsealed bags will be contained in an EVA transfer liner, one for each EVA.The EVA transfer liners will be contained in a soft-goods container.
- If the outer box opened, all samples would still be in their individual containers and the EVA liners.
- If the outer box opened AND an EVA liner bag split open, all samples would be in their individual containers.
- If the outer box opened AND an EVA liner bag split open AND an individual bag opened, then only that amount would be spilled, which is a maximum 2 kg of regolith.

Sealed containers:

- Sealed containers are drive tubes and PSCs that contain bulk regolith.
- Sealed containers will be returned in a Secondary Sealed container.
- If the Secondary Sealed container opened, all samples would be contained in their primary container.
- If the Secondary Sealed container opened AND a primary container opened, then only that amount would be spilled, which is a maximum 1 kg of regolith.

Volatile release based on full release from total sample mass:

- Vapor density (molecular mass based on fractional abundances) = 0.641 g/L at STP
- Total volume 1.23 L (at STP)
- Total pressure 1.54E4 Pa (assuming 8L return container)

Species	Molar mass (g/mol)	Vapor Density (g/L at STP)	Concentration (cc/g)	Total abundance (cc)
H_2	2	0.089	5.76E-03	2.74E+02
^{4}He	4	0.178	1.15E-04	5.47E+00
^{20}Ne	20	0.892	2.76E-07	1.31E-02
^{40}Ar	40	1.785	2.75E-07	1.30E-02
N_2	28	1.249	1.90E-07	9.03E-03
Water	18	0.803	2.00E-02	9.50E+02
CO_2	46	2.052	2.00E-07	9.50E-03
			2.59E-02	**1.23E+03**

APPENDIX C
REFERENCES

Anand M. (2011) Lunar Water: A Brief Review. *Earth, Moon, and Planets* **107**(1), 65-73.

Ando J., Li S., Robinson M., and Wagner R. (2025) Radiance Contrasts at Possible Lunar Water Ice Exposures Seen by ShadowCam. *The Planetary Science Journal* **6**(3), 62.

Benna M., Hurley D. M., Stubbs T. J., Mahaffy P. R., and Elphic R. C. (2019) Lunar soil hydration constrained by exospheric water liberated by meteoroid impacts. *Nature Geoscience* **12**(5), 333-338.

Benna M., Mahaffy P. R., Halekas J. S., Elphic R. C., and Delory G. T. (2015) Variability of helium, neon, and argon in the lunar exosphere as observed by the LADEE NMS instrument. *Geophysical Research Letters* **42**(10), 3723-3729.

Boazman S. J., Shah J., Harish, Gawronska A. J., Halim S. H., Satyakumar A. V., Gilmour C. M., Bickel V. T., Barrett N., and Kring D. A. (2022) The Distribution and Accessibility of Geologic Targets near the Lunar South Pole and Candidate Artemis Landing Sites. *The Planetary Science Journal* **3**(12), 275.

Campbell B. A., Campbell D. B., Chandler J. F., Hine A. A., Nolan M. C., and Perillat P. J. (2003) Radar imaging of the lunar poles. *Nature* **426**, 137-138.

Cannon K. M. and Britt D. T. (2020) A geologic model for lunar ice deposits at mining scales. *Icarus* **347**, 113778.

Cannon K. M., Deutsch A. N., Head J. W., and Britt D. T. (2020) Stratigraphy of Ice and Ejecta Deposits at the Lunar Poles. *Geophysical Research Letters* **47**(21), e2020GL088920.

Carrier W. D. (2003) Particle Size Distribution of Lunar Soil. *Journal of Geotechnical and Geoenvironmental Engineering* **129**(10), 956-959.

Casanova S., Espejel C., Dempster A. G., Anderson R. C., Caprarelli G., and Saydam S. (2020) Lunar polar water resource exploration – Examination of the lunar cold trap reservoir system model and introduction of play-based exploration (PBE) techniques. *Planetary and Space Science* **180**, 104742.

Chabot N. L., Ernst C. M., Denevi B. W., Harmon J. K., Murchie S. L., Blewett D. T., Solomon S. C., and Zhong E. D. (2012) Areas of permanent shadow in Mercury's south polar region ascertained by MESSENGER orbital imaging. *Geophysical Research Letters* **39**(9).

Clark R. N. (2009) Detection of adsorbed water and hydroxyl on the Moon. *Science* **326**(5952), 562-4.

Colaprete A., Schultz P., Heldmann J., Wooden D., Shirley M., Ennico K., Hermalyn B., Marshall W., Ricco A., Elphic R. C., Goldstein D., Summy D., Bart G. D., Asphaug E., Korycansky D., Landis D., and Sollitt L. (2010) Detection of Water in the LCROSS Ejecta Plume. *Science* **330**, DOI: 10.1126/science.1186986.

Costello E. S., Ghent R. R., and Lucey P. G. (2021) Secondary Impact Burial and Excavation Gardening on the Moon and the Depth to Ice in Permanent Shadow. *Journal of Geophysical Research: Planets* **126**(9), e2021JE006933.

Crites S., Lucey P., and Lawrence D. (2011) In-situ production of organic molecules at the poles of the Moon. *AGUFM. P13D1730C*.

Curran N. M., Nottingham M., Alexander L., Crawford I. A., Füri E., and Joy K. H. (2020) A database of noble gases in lunar samples in preparation for mass spectrometry on the Moon. *Planetary and Space Science* **182**, 104823.

Dartnell L. R. (2011) Ionizing radiation and life. *Astrobiology* **11**(6), 551-582.

Denevi B. W., Noble S. K., Christoffersen R., Thompson M. S., Glotch T. D., Blewett D. T., Garrick-Bethell I., Gillis-Davis J. J., Greenhagen B. T., Hendrix A. R., Hurley D. M., Keller L. P., Kramer G. Y., and Trang D. (2023) Space Weathering At The Moon. *Reviews in Mineralogy and Geochemistry* **89**(1), 611-650.

Deutsch A. N., Chabot N. L., Mazarico E., Ernst C. M., Head J. W., Neumann G. A., and Solomon S. C. (2016) Comparison of areas in shadow from imaging and altimetry in the north polar region of Mercury and implications for polar ice deposits. *Icarus* **280**, 158-171.

Deutsch A. N., Head J. W., and Neumann G. A. (2020) Analyzing the ages of south polar craters on the Moon: Implications for the sources and evolution of surface water ice. *Icarus* **336**, 113455.

Farrell W. M., Hurley D. M., Poston M. J., Hayne P. O., Szalay J. R., and McLain J. L. (2019) The Young Age of the LAMP-observed Frost in Lunar Polar Cold Traps. *Geophysical Research Letters* **46**(15), 8680-8688.

Feldman W. C., Lawrence D. J., Elphic R. C., Barraclough B. L., Maurice S., Genetay I., and Binder A. B. (2000) Polar hydrogen deposits on the Moon. *Journal of Geophysical Research* **105**, 4175-4196.

Feldman W. C., Maurice S., Lawrence D. J., Little R. C., Lawson S. L., Gasnault O., Wiens R. C., Barraclough B. L., Elphic R. C., Prettyman T. H., Steinberg J. T., and Binder A. B. (2001) Evidence for water ice near the lunar poles. *Journal of Geophysical Research* **106**, 23231-23252.

Fisher E. A., Lucey P. G., Lemelin M., Greenhagen B. T., Siegler M. A., Mazarico E., Aharonson O., Williams J.-P., Hayne P. O., Neumann G. A., Paige D. A., Smith D. E., and Zuber M. T. (2017) Evidence for surface water ice in the lunar polar regions using reflectance measurements from the Lunar Orbiter Laser Altimeter and temperature measurements from the Diviner Lunar Radiometer Experiment. *Icarus* **292**, 74-85.

Flory D. A. and Simoneit B. R. (1972) Terrestrial contamination in Apollo lunar samples. *Space life sciences* **3**(4), 457-468.

Gibson E. K. and Andrawes F. (1978) Nature of the Gas Phases Released from Lunar Rocks and Soils upon Crushing. In *Lunar and Planetary Science Conference*, pp. 379-381. Lunar and Planetary Institute, Houston.

Graf J. C. (1993) Lunar soils grain size catalog. *NASA Technical Report* **NASA-RP-1265**, 484.

Gross J., Zeigler R. A., Mosie A. B., Krysher C., Eckley S. A., Ketcham R. A., Hanna R. D., Edey D., Kent J. J., McCubbin F. M., McDonald F., Schild T., Lucey P. G., Sun L., Flom A., Parai R., Meshik A., Pravdivtseva O., Petro N. E., Shearer C. K., and the A. S. T. (2025) Apollo Next Generation Sample Analysis (ANGSA) Samples: Preliminary Examination of Double Drive Tube Samples 73001 and 73002 and Lessons Learned for Returning to the Moon With Artemis. *Journal of Geophysical Research: Planets* **130**(1), e2024JE008585.

Hayne P. O., Aharonson O., and Schörghofer N. (2021) Micro cold traps on the Moon. *Nature Astronomy* **5**(2), 169-175.

Hayne P. O., Hendrix A., Sefton-Nash E., Siegler M. A., Lucey P. G., Retherford K. D., Williams J.-P., Greenhagen B. T., and Paige D. A. (2015) Evidence for exposed water ice in the Moon's south polar regions from Lunar Reconnaissance Orbiter ultraviolet albedo and temperature measurements. *Icarus* **255**, 58-69.

Heber V. S., McKeegan K. D., Steele R. C. J., Jurewicz A. J. G., Rieck K. D., Guan Y., Wieler R., and Burnett D. S. (2021) Elemental Abundances of Major Elements in the Solar Wind as Measured in Genesis Targets and Implications on Solar Wind Fractionation. *The Astrophysical Journal* **907**(1), 15.

Heiken G. H., Vaniman D. T., and French B. M. (1991) The Lunar Sourcebook: A User's Guide to the Moon, pp. 736. Cambridge University Press, Cambridge.

Heldmann J. L., Colaprete A., Wooden D. H., Ackermann R. F., Acton D. D., Backus P. R., Bailey V., Ball J. G., Barott W. C., Blair S. K., Buie M. W., Callahan S., Chanover N. J., Choi Y.-J., Conrad A., Coulson D. M., Crawford K. B., DeHart R., de Pater I., Disanti M., Forster J. R., Furusho R., Fuse T., Geballe T., Gibson J. D., Goldstein D., Gregory S. A., Gutierrez D. J., Hamilton R. T., Hamura T., Harker D. E., Harp G. R., Haruyama J., Hastie M., Hayano Y., Hinz P., Hong P. K., James S. P., Kadono T., Kawakita H., Kelley M. S., Kim D. L., Kurosawa K., Lee D.-H., Long M., Lucey P. G., Marach K., Matulonis A. C., McDermid R. M., McMillan R., Miller C., Moon H.-K., Nakamura R., Noda H., Okamura N., Ong L., Porter D., Puschell J. J., Rayner J. T., Rembold J. J., Roth K. C., Rudy R. J., Russell R. W., Ryan E. V., Ryan W. H., Sekiguchi T., Sekine Y., Skinner M. A., Sôma M., Stephens A. W., Storrs A., Suggs R. M., Sugita S., Sung E.-C., Takatoh N., Tarter J. C., Taylor S. M., Terada H., Trujillo C. J., Vaitheeswaran V., Vilas F., Walls B. D., Watanabe J.-i., Welch W. J., Woodward C. E., Yim H.-S., and Young E. F. (2012) LCROSS (Lunar Crater Observation and Sensing Satellite) Observation Campaign: Strategies, Implementation, and Lessons Learned. *Space Science Reviews* **167**(1), 93-140.

Hodges C. A. and Muehlberger W. R. (1981) Geology of the Apollo 16 area, Central Lunar Highlands. In *Professional Paper* (ed. G. E. Ulrich).

Hodges Jr. R. R. (2016) Methane in the lunar exosphere: Implications for solar wind carbon escape. *Geophysical Research Letters* **43**(13), 6742-6748.

Hodges R. R. (2002) Ice in the lunar polar regions revisited. *Journal of Geophysical Research* **107**(E2), 5011--7.

Kleinhenz J., McAdam A., Colaprete A., Beaty D., Cohen B., Clark P., Gruener J., Schuler J., and Young K. (2020) Lunar Water ISRU Measurement Study (LWIMS): Establishing a Measurement Plan for Identification and Characterization of a Water Reserve. *NASA Technical Memorandum* **20205008626**.

Kovtun R. N., Gruener J. E., and Slabic A. (2024) Coarsening Up: Expanding the Particle Size Distribution of Lunar Simulants to Encompass a Comprehensive Range of Regolith Granularity. In *Lunar and Planetary Science Conference*, pp. 2758.

Li S., Lucey P. G., Milliken R. E., Hayne P. O., Fisher E., Williams J.-P., Hurley D. M., and Elphic R. C. (2018) Direct evidence of surface exposed water ice in the lunar polar regions. *Proceedings of the National Academy of Sciences* **115**(36), 8907.

Liu Y., Guan Y., Zhang Y., Rossman G. R., Eiler J. M., and Taylor L. A. (2012) Direct measurement of hydroxyl in the lunar regolith and the origin of lunar surface water. *Nature Geoscience* **5**, 779.

Livengood T. A., Mitrofanov I. G., Chin G., Boynton W. V., Bodnarik J. G., Evans L. G., Harshman K. P., Litvak M. L., McClanahan T. P., Sagdeev R. Z., Sanin A. B., Starr R. D., and Su J. J. (2018) Background and lunar neutron populations detected by LEND and average concentration of near-surface hydrogen near the Moon's poles. *Planetary and Space Science* **162**, 89-104.

Lucey P. G., Petro N., Hurley D. M., Farrell W. M., Prem P., Costello E. S., Cable M. L., Barker M. K., Benna M., Dyar M. D., Fisher E. A., Green R. O., Hayne P. O., Hibbitts K., Honniball C., Li S., Malaret E., Mandt K., Mazarico E., McCanta M., Pieters C., Sun X., Thompson D., and Orlando T. (2022) Volatile interactions with the lunar surface. *Geochemistry* **82**(3), 125858.

McKay D. S., Fruland R. M., and Heiken G. H. (1974) Grain size and the evolution of the lunar soils. *Proceedings of the Lunar Science Conference* **5th**(1), 887-906.

McKay D. S., Heiken G., Basu A., Blanford G., Simon S., Reedy R., French B. M., and Papike J. (1991) The lunar regolith. In *Lunar Sourcebook* (eds. G. H. Heiken, D. T. Vaniman, and B. M. French), pp. 285-356. Cambridge University Press, Cambridge, UK.

Mitrofanov I. G., Sanin A. B., and Litvak M. L. (2016) Water in the Moon's polar areas: Results of LEND neutron telescope mapping. *Doklady Physics* **61**(2), 98-101.

Nozette S., Lichtenberg C. L., Spudis P., Bonner R., Ort W., Malaret E., Robinson M., and Shoemaker E. M. (1996) The Clementine Bistatic Radar Experiment. *Science* **274**, 1495-1498.

Paige D. A., Siegler M. A., Zhang J. A., Hayne P. O., Foote E. J., Bennett K. A., Vasavada A. R., Greenhagen B. T., Schofield J. T., McCleese D. J., Foote M. C., DeJong E., Bills B. G., Hartford W., Murray B. C., Allen C. C., Snook K., Soderblom L. A., Calcutt S., Taylor F. W., Bowles N. E., Bandfield J. L., Elphic R., Ghent R., Glotch T. D., Wyatt M. B., and Lucey P. G. (2010) Diviner Lunar Radiometer observations of cold traps in the Moon's south polar region. *Science* **330**(6003), 479-82.

Parai R., Rodriguez J., Patzkowsky S., Solari N., Woody K. A., Meshik A., Pravdivtseva O., Jolliff B. L., Shearer C. K., Sharp Z. D., Cassata W., Zeigler R., Gross J., McCubbin F. M., McDonald F., and ANGSA Team (2022) Noble Gas Isotopes in the Apollo 17 73001 Core Sample Vacuum Container Gas. In *Lunar and Planetary Science Conference*, pp. 2028.

Pieters C. M., Goswami J. N., Clark R. N., Annadurai M., Boardman J., Buratti B., Combe J. P., Dyar M. D., Green R., Head J. W., Hibbitts C., Hicks M., Isaacson P., Klima R., Kramer G., Kumar S., Livo E., Lundeen S., Malaret E., McCord T., Mustard J., Nettles J., Petro N., Runyon C., Staid M., Sunshine J., Taylor L. A., Tompkins S., and Varanasi P. (2009) Character and spatial distribution of OH/H2O on the surface of the Moon seen by M3 on Chandrayaan-1. *Science* **326**(5952), 568-72.

Sanin A. B., Mitrofanov I. G., Litvak M. L., Bakhtin B. N., Bodnarik J. G., Boynton W. V., Chin G., Evans L. G., Harshman K., Fedosov F., Golovin D. V., Kozyrev A. S., Livengood T. A., Malakhov A. V., McClanahan T. P., Mokrousov M. I., Starr R. D., Sagdeev R. Z., Tret'yakov V. I., and Vostrukhin A. A. (2017) Hydrogen distribution in the lunar polar regions. *Icarus* **283**, 20-30.

Sanin A. B., Mitrofanov I. G., Litvak M. L., Malakhov A., Boynton W. V., Chin G., Droege G., Evans L. G., Garvin J., Golovin D. V., Harshman K., McClanahan T. P., Mokrousov M. I., Mazarico E., Milikh G., Neumann G., Sagdeev R., Smith D. E., Starr R. D., and Zuber M. T. (2012) Testing lunar permanently shadowed regions for water ice: LEND results from LRO. *Journal of Geophysical Research (Planets)* **117**.

Sharp Z. D., Shearer C. K., Meshik A., Parai R., Pravdivtseva O., Cassata W., Gross J., McCubbin F., Zeigler R., Jolliff B. L., and McDonald F. (2022) Major Element Gas Composition of the Apollo 73001 Inner (CSVC) and Outer Containers. *Apollo 17-ANGSA Workshop*, #2052.

Siegler M., Miller R. S., Keane J. T., Laneuville M., Paige D. A., Matsuyama I., Lawrence D. J., Crotts A., and Poston M. J. (2016) Lunar true polar wander inferred from polar hydrogen. *Nature* **531**(7), 480--484.

Spudis P. D., Bussey B., Plescia J., Josset J.-L., and Beauvivre S. (2008) Geology of Shackleton Crater and the south pole of the Moon. *Geophysical Research Letters* **35**(14).

Sunshine J. M., Farnham T. L., Feaga L. M., Groussin O., Merlin F., Milliken R. E., and A'Hearn M. F. (2009) Temporal and spatial variability of lunar hydration as observed by the Deep Impact spacecraft. *Science* **326**(5952), 565-8.

Szalay J. R., Pokorný P., Horányi M., Janches D., Sarantos M., and Srama R. (2019) Impact ejecta environment of an eccentric asteroid: 3200 Phaethon. *Planetary and Space Science* **165**, 194-204.

Walker R. M. (1975) Interaction of energetic nuclear particles in space with the lunar surface. *Annual Review of Earth and Planetary Sciences* **3**(1), 99-128.

Weber R. C., Lawrence S. J., Cohen B. A., Boyce J. W., Collier M. R., Fagan A. L., Fassett C. I., Gaddis L., Gross J., Gruener J. E., Heldmann J. L., Pieters C. M., Petro N., and Young K. E. (2020) The Artemis III Science Definition Team Report. *https://www.nasa.gov/sites/default/files/atoms/files/artemis-iii-science-definition-report-12042020c.pdf*.

Wieler R. (1998) The solar noble gas record in lunar samples and meteorites. *Space Science Reviews* **85**(1-2), 303-314.

Wieler R. (2016) Do lunar and meteoritic archives record temporal variations in the composition of solar wind noble gases and nitrogen? A reassessment in the light of Genesis data. *Chemie der Erde* **76**, 463-480.

Zhang J. A. and Paige D. A. (2009) Cold-trapped organic compounds at the poles of the Moon and Mercury: Implications for origins. *Geophysical Research Letters* **36**(16).